

WAVE DISPERSION CHARACTERISTICS IN 1D METAMATERIAL SYSTEMS

ABHIGNA BHATT



**DEPARTMENT OF CIVIL ENGINEERING
INDIAN INSTITUTE OF TECHNOLOGY DELHI
JANUARY 2025**

© Indian Institute of Technology Delhi (IITD), New Delhi, 2025

Wave Dispersion Characteristics in 1D Metamaterial Systems

by

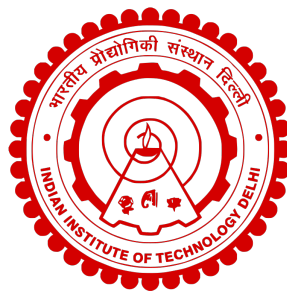
Abhigna Bhatt

Department of Civil Engineering

Submitted

in fulfillment of the requirements of the degree of Doctor of Philosophy

to the



INDIAN INSTITUTE OF TECHNOLOGY DELHI

JANUARY 2025

CERTIFICATE

This is to certify that the thesis titled **Wave dispersion characteristics in 1D meta-material systems**, submitted by **Ms. Bhatt Abhigna Sandipkumar**, to the Indian Institute of Technology, Delhi, for the award of the degree of **Doctor of Philosophy**, is a bonafide record of the research work done by her under our supervision and guidance. The contents of this thesis, in full or in parts, have not been submitted to any other Institute or University for the award of any degree or diploma.

Dr. Arnab Banerjee
Assistant Professor
Dept. of Civil Engineering
IIT Delhi, 110016

New Delhi
January, 2025.

ACKNOWLEDGEMENTS

The journey to a PhD is often an unexpected adventure, filled with twists, turns, challenges, and a few roadblocks. Such a demanding and transformative experience becomes achievable only with a strong support system, and I am deeply grateful to all those who stood by me during this journey.

First and foremost, I extend my heartfelt gratitude to my supervisor and mentor, Prof. Arnab Banerjee, for believing in me and guiding me through every step of this path. Under his mentorship, I not only grew as a researcher but also learned invaluable life lessons while being part of the incredible work culture he fostered at MMMES Lab (Metalab). I am immensely thankful to Prof. Sondipan Adhikari from the University of Glasgow for his insightful guidance and for providing me with the opportunity to present my work at the University of Glasgow. My sincere thanks also go to Dr. Kamal Krishna Bera for his collaboration in my research, which significantly enhanced my paper-writing skills.

I am deeply grateful to my meta friends, particularly Somya Ranjan Patro, for collaborating in my research and always being so supportive. My appreciation extends to Rishab and Arindam for the enriching discussions that broadened my perspective on research. A special thanks to Shivam for his help with 3D printing the experimental models.

The camaraderie and unwavering support of my Metafamily members: Susmita, Satyendra, Iqra, Sudip, Muskaan, Namrata, Pranay, Indrajit, Souryadeep, Somraj, Mayuresh, Tonmoy, Bhavana, Somendu, Daniel, Ajinkya, and Rajan have been incredible and unforgettable. Thank you all for making this journey both intellectually stimulating and filled with joy. I am also grateful to Deveshji for assisting with experimental setups and management tasks. A special thanks to Atri Ma'am for her invaluable support, care, and boundless energy during our celebrations, big or small.

Embarking on motherhood during my second year of PhD was one of the most challenging

phases of my life, both professionally and personally. My deepest gratitude goes to my family for their unwavering support during this time. My heartfelt thanks to my mother-in-law, Amita Poddar, and father-in-law, Ramanuj Poddar, as well as to my parents, Hetal Bhatt and Sandip Bhatt, and my sister, Atixa, for their love, selflessness, and encouragement.

Finally, no words can adequately express my gratitude to my life partner, Divyaprakash, whose support, motivation, and unwavering belief in me have been my pillars of strength. You have been my constant source of confidence and courage. To our son, Rudransh, now two years old, thank you for being such an amazing child and for bringing endless joy to my toughest days.

I also bow my head in gratitude to the Almighty for all the blessings, both known and unknown, that have guided me through this journey.

(Abhigna Bhatt)

ABSTRACT

Over the past few decades, the study of flexural wave propagation through metamaterials has garnered significant attention due to their remarkable wave manipulation capabilities. Depending on the characteristics of the representative unit cell, metamaterials can either facilitate or inhibit wave propagation within certain frequency bands, making them highly applicable in fields such as vibration isolation, energy harvesting, wave filtering, and sound insulation. Despite these advances, substantial research opportunities remain in the analytical solutions of wave dispersion in metamaterials with various mechanisms and configurations.

This study presents analytical solutions for wave dispersion characteristics in one-dimensional metamaterial systems, ranging from simple to complex configurations, including discrete monocoupled systems, discrete multicoupled systems, continuous multicoupled systems, and continuous nonlinear systems.

First, a generalized monocoupled system is introduced, combining elements with inertial amplification, negative mass, and negative stiffness. A hierarchical stiffness system is conceptualized to produce multiple attenuation peaks. A general framework employing rational polynomials is developed, from which closed-form expressions for the positions of attenuation peaks and bounding frequencies of propagation bands can be derived for any undamped monocoupled system.

The study also explores wave dispersion in a discrete bicoupled system formed by coupling two spring-mass chains, analyzed for both straight and zigzag couplings. The analytical dispersion relation is derived using the dynamic stiffness matrix and the Bloch-Floquet theorem, with invariants characterizing the band structure. Mechanisms of band veering and locking are examined, identifying a maxon at wave locking and a roton at unlocking in the zigzag coupling. Sensitivity analysis on the invariant plane reveals how various parameters influence wave propagation characteristics.

For continuous systems, the study investigates flexural wave propagation through a rigid elastic combined metabeam (RECM) considering the finite dimensions of the rigid mass. The rotary inertia of the rigid body introduces a local resonance (LR) band, which can bridge the gap between two Bragg scattering (BS) bands, resulting in an ultra-wide stop band for specific combinations of governing non-dimensional parameters. Additionally, a vibration isolator device based on the rigid elastic combined beam is developed, exhibiting a wide bandgap due to double antiresonance peaks, with experimental validation of the isolator conducted. A parametric study varying the geometric properties of the rigid elastic isolator system enhances the understanding of bandgap and attenuation characteristics within the attenuation band. Furthermore, wave dispersion in a chain of masses connected with a designed rigid elastic isolator is studied and validated, with analytical solutions obtained through the transmittance study of the representative unit cell.

Lastly, for continuous nonlinear systems, the amplitude-dependent dispersion relation of a damped beam supported by nonlinear springs is studied, considering both softening and hardening cubic nonlinearities along with viscous and strain rate damping. Using a multiscale method, the wave dispersion equation is analytically derived and validated against numerical results. The research provides closed-form equations for frequency shifts in undamped systems due to nonlinearities and time-dependent dispersion in damped systems.

सार

पिछले कुछ दशकों में, मेटामटेरियल के माध्यम से फ्लेक्सुरल तरंग प्रसार के अध्ययन ने उनकी उल्लेखनीय तरंग हेरफेर क्षमताओं के कारण महत्वपूर्ण ध्यान आकर्षित किया है। प्रतिनिधि इकाई सेल की विशेषताओं के आधार पर, मेटामटेरियल कुछ आवृत्ति बैंड के भीतर तरंग विक्षेपण को सुविधाजनक या बाधित कर सकते हैं, जिससे वे कंपन पृथक्करण, ऊर्जा संचयन, तरंग फ़िल्टरिंग और ध्वनि पृथक्करण जैसे क्षेत्रों में अत्यधिक लागू होते हैं। इन प्रगति के बावजूद, विभिन्न तंत्रों और विन्यासों के साथ मेटामटेरियल में तरंग विक्षेपण के विश्लेषणात्मक समाधानों में पर्याप्त शोध के अक्सर बने हुए हैं।

यह अध्ययन एक-आयामी मेटामटेरियल प्रणालियों में तरंग विक्षेपण विशेषताओं के लिए विश्लेषणात्मक समाधान प्रस्तुत करता है, जो सरल से जटिल विन्यासों तक फैले हुए हैं, जिनमें विविक्त मोनो-कपल्ल प्रणालियाँ, विविक्त मल्टी-कपल्ल प्रणालियाँ, सतत मल्टी-कपल्ल प्रणालियाँ और सतत गैर-रैखिक प्रणालियाँ शामिल हैं।

पहले, एक सामान्यीकृत मोनो-कपल्ल प्रणाली प्रस्तुत की गई है, जिसमें जड़त्वीय प्रवर्धन, नकारात्मक द्रव्यमान और नकारात्मक कठोरता वाले तत्वों को संयोजित किया गया है। बहु-क्षीणन शिखरों को उत्पन्न करने के लिए एक श्रेणीबद्ध कठोरता प्रणाली की कल्पना की गई है। एक सामान्य रूपरेखा विकसित की गई है, जिसमें युक्तिसंगत बहुपदों (रैशनल पॉलिनोमियल्स) का उपयोग किया गया है, जिससे किसी भी अनडैम्पड मोनो-कपल्ल प्रणाली के लिए क्षीणन शिखरों की स्थितियों और विक्षेपण बैंड की सीमित आवृत्तियों के लिए बंद-रूप अभिव्यक्तियाँ प्राप्त की जा सकती हैं।

अध्ययन में तरंग विक्षेपण का विश्लेषण एक विविक्त बाइ-कपल्ल प्रणाली में भी किया गया है, जिसे दो स्पिंग-द्रव्यमान श्रृंखलाओं को संयोजित करके बनाया गया है। इस प्रणाली का विश्लेषण सीधा और ज़िगज़ैग दोनों प्रकार के संयोजनों के लिए किया गया है। विश्लेषणात्मक विक्षेपण संबंध को गतिशील कठोरता मैट्रिक्स और ब्लॉक-फ्लॉके थ्योरम का उपयोग करके व्युत्पन्न किया गया है, जिसमें बैंड संरचना को विशेषता प्रदान करने वाले अपरिवर्तनीय (इनवेरिएंट्स) शामिल हैं। बैंड वीयरिंग और लॉकिंग की प्रक्रियाओं की जांच की गई है, जिसमें ज़िगज़ैग कपलिंग में वेव लॉकिंग के दौरान एक मैक्सॉन और अनलॉकिंग के दौरान एक रॉटॉन की पहचान की गई है। अपरिवर्तनीय तल (इनवेरिएंट प्लेन) पर की गई संवेदी विश्लेषण (सेंसिटिविटी एनालिसिस) यह प्रकट करती है कि विभिन्न मापदंड तरंग विक्षेपण विशेषताओं को कैसे प्रभावित करते हैं।

सतत प्रणालियों के संदर्भ में, यह अध्ययन एक कठोर-लोचदार संयुक्त मेटाबीम (RECM) के माध्यम से फ्लेक्सुरल तरंग विक्षेपण की जांच करता है, जिसमें कठोर द्रव्यमान के सीमित आयामों को ध्यान में रखा गया है। कठोर पिंड का घूर्णी जड़त्व (रोटरी इनर्शिया) एक स्थानीय अनुनाद (LR) बैंड को उत्पन्न करता

है, जो दो ब्रेग प्रकीर्णन (BS) बैंड के बीच की दूरी को पाट सकता है, जिससे गैर-आयामी (नॉन-डाइमेंशनल) मापदंडों के विशिष्ट संयोजनों के लिए एक अत्यधिक विस्तृत स्टॉप बैंड बनता है। इसके अतिरिक्त, कठोर-लोचदार संयुक्त बीम पर आधारित एक कंपन पृथक्करण उपकरण विकसित किया गया है, जो दोहरे प्रत्यानुनाद (एंटीरेज़ोनेंस) शिखरों के कारण एक विस्तृत बैंडगैप प्रदर्शित करता है, और इस पृथक्करण प्रणाली का प्रायोगिक सत्यापन किया गया है। कठोर-लोचदार पृथक्करण प्रणाली के ज्यामितीय गुणों को परिवर्तित करके किए गए पैरामीट्रिक अध्ययन से बैंडगैप और क्षीणन बैंड के भीतर क्षीणन विशेषताओं की समझ को बेहतर बनाया गया है। इसके अतिरिक्त, एक श्रृंखला में संयोजित कठोर-लोचदार पृथक्करण प्रणाली के माध्यम से द्रव्यमानों के बीच तरंग विक्षेपण का अध्ययन और सत्यापन किया गया है, जहाँ विश्लेषणात्मक समाधान प्रतिनिधि इकाई सेल के प्रसारण अध्ययन (ट्रांसमिटेस स्टडी) के माध्यम से प्राप्त किए गए हैं।

अंततः, सतत गैर-रैखिक प्रणालियों के लिए, एक अवमंदित (डैम्पड) बीम, जिसे गैर-रैखिक स्प्रिंग्स द्वारा समर्थित किया गया है, की आयाम-निर्भर विक्षेपण संबंध का अध्ययन किया गया है। इसमें कोमलन (सॉफ्टनिंग) और कठोरन (हार्डनिंग) प्रकार की घनात्मक (क्यूबिक) गैर-रैखिकताओं के साथ-साथ श्यान (विस्कस) और तनाव-दर (स्ट्रेन रेट) अवमंदन को भी शामिल किया गया है। बहु-स्केल विधि का उपयोग करके, तरंग विक्षेपण समीकरण का विश्लेषणात्मक रूप से व्युत्पादन किया गया है और इसे संख्यात्मक परिणामों के साथ सत्यापित किया गया है। यह शोध अनडैम्पड प्रणालियों में गैर-रैखिकताओं के कारण आवृत्ति परिवर्तनों और डैम्पड प्रणालियों में समय-आश्रित विक्षेपण के लिए बंद-रूप समीकरण प्रदान करता है।

Contents

CERTIFICATE	i
ACKNOWLEDGEMENTS	ii
ABSTRACT	iv
List of figures	xx
List of tables	xxi
Abbreviations	xxii
List of symbols	xxiii
1 Introduction	1
1.1 Metamaterials	1
1.2 Aim	2
1.3 Objectives	2
1.4 Thesis organization	2
2 Literature review	5
2.1 Waves in 1D metamaterials	5
2.1.1 History of wave dispersion in metamaterials	5
2.1.2 Classification of representative unit cell	7
2.2 Dispersion phenomena based on types of unit cells	9
2.2.1 Linear monocoupled metamaterials	9
2.2.2 Linear discrete multicoupled metamaterials	14
2.2.3 Linear continuous multicoupled metamaterials	18

2.2.4	Nonlinear metamaterials	22
2.3	Motivation and Research Gap	25
3	Wave characteristics in monocoupled systems	27
3.1	The generalised mono-coupled system: Conceptualization	27
3.1.1	Equation of motion of each mass	28
3.1.2	Compatibility equation	30
3.1.3	Construction of Dynamic Stiffness Matrix	31
3.1.4	A general theory of attenuation characteristics in monocoupled system	33
3.1.5	Non-Dimensional form and various mono coupled systems	36
3.1.6	Peak in attenuation level and bounds of propagation band	36
3.1.7	Validation	40
3.1.8	Results and Discussions	42
3.1.9	Inertial amplifier negative mass negative stiffness (IANMNS)	42
3.1.10	Inertial amplifier negative mass negative stiffness (IANMNS) special case	43
3.1.11	Negative mass negative stiffness (NMNS)	44
3.1.12	Inertial amplifier negative mass (IANM)	45
3.1.13	Summary	46
3.1.14	Conclusion	49
3.2	Hierarchical stiffness metamaterial	50
3.2.1	Conceptualization of the hierarchical stiffness metamaterial	50
3.2.2	Mathematical modelling for N level hierarchical stiffness metamaterial (HSM)	52
3.2.3	Identification of the attenuation characteristics (attenuation peaks and bounds)	56
3.2.4	Results and discussions	57
3.2.5	Conclusion	63
4	Wave characteristics in multicoupled discrete systems	64
4.1	A discrete bicoupled system: Conceptualization	64
4.2	Methodology	66
4.2.1	The general wave dispersion equation	67

4.2.2	Characteristics of wave dispersion in Bicoupled system	69
4.3	Validation	74
4.4	Results and Discussions	76
4.5	Conclusion	82
5	Wave characteristics in multicoupled systems	86
5.1	Methodology	87
5.1.1	Governing equation	87
5.1.2	Spectral element formulation	88
5.1.3	Dispersion relation	91
5.1.4	Frequency domain response of Finite RECM system	92
5.1.5	Visualisation of wave propagation in space and time	92
5.2	Validation	93
5.3	Results and Discussion	96
5.3.1	Study of the dispersion characteristics and natural frequencies	96
5.3.2	Visualization of wave propagation	99
5.4	Conclusion	101
6	Vibration control system using RECM	110
6.1	Analysis of unit cell of rigid elastic vibration isolator	111
6.1.1	Theoretical analysis and design of REVI	112
6.1.2	Estimation of rotational stiffness	123
6.1.3	Estimation of vibration isolation performance	128
6.1.4	Results and discussions	131
6.2	Wave dispersion study in periodically connected REVI	137
6.2.1	Results and Discussions	138
6.2.2	Conclusion	143
7	Wave characteristics in nonlinear metamaterials	145
7.1	Methodology	145
7.1.1	Governing equation	146
7.1.2	Multiple scales Method	146
7.1.3	Finite element modelling	150

7.2	Results and discussion	152
7.2.1	Numerical validation	152
7.2.2	Undamped system	159
7.2.3	Damped system	161
7.3	Summary and Conclusion	163
8	Conclusions and suggestions for future research	166
8.1	Conclusions	166
8.2	Future scope of work	167
	References	187
	Publications	188
	Curriculum Vitae	190

List of Figures

2.1	Classification of representative unit cell.	8
2.2	Comparing dispersion relation plot of monoatomic monocoupled chain in (a) with different established mechanisms such as (b) Basic spring mass system, (c) Inertial amplification mechanism, (d) negative mass mechanism, and (e) negative stiffness mechanism.	11
2.3	Comparing dispersion relation plot of monocoupled chain with combined mechanisms mechanisms such as (a) Inertial amplification with negative mass mechanism [1], (b) negative mass with negative stiffness mechanism [2] and (c) illustrates the dispersion plots.	13
2.4	(a) Monocoupled chain with hierarchical mass in mass system (b) dispersion plot of mass in mass hierarchical chain [3].	14
2.5	Roton-like acoustic dispersion in 1D acoustic metamaterials with third and second-nearest-neighbor interactions, (a) 1D model illustrates third-nearest-neighbor interactions K_3 (purple lines), second nearest neighbour interactions k_2 (blue lines) and with nearest-neighbor interactions K_1 represented by red springs, (b) The dispersion relation is plotted as propagation constant (κ) versus excitation frequency (ω), and (c) the corresponding group velocity of the studied metamaterials are presented [4].	16
2.6	One-dimensional isomer models: (a) A monocoupled meta chain with hierarchical resonators, (c) a discrete multicoupled resonant metachain with straight connections, and (e) a discrete multicoupled resonant metachain with zigzag connections. (b, d, f) show the band structures corresponding to the isomers in (a, c, e), respectively [5]. The pink shaded region illustrates the attenuation band.	18
2.7	(a) Euler Bernoulli beam, (c) Beam with alternating material properties, (e) Beam with alternating geometric properties, (g) Beam with spring supports, (i) Beam with resonators, and (b,d,f,h,i) shows their respective band structures.[6].	20
2.8	(a) Monoatomic nonlinear spring mass system, (b) Amplitude dependant dispersion plot for different nonlinear stiffness [7],(c) Nonlinear spring mass system on nonlinear foundation, and (d) quasi-static band gap with amplitude based tunability [8].	24

3.1	(a) Periodically connected infinitely long chain of IANMNS system, (b) Nodal degrees of freedom of IANMNS system.	28
3.2	(a) Generalised monocoupled system Inertial Amplifier Negative Mass Negative Stiffness (IANMNS) (b) Inertial Amplifier Negative Stiffness (IANS) system obtained by considering $m_1 = 0$, (c) Negative Mass Negative Stiffness (NMNS) system obtained by considering $m_a = 0$, (d) Negative Stiffness (NS) system obtained by considering $m_a = 0$ and $m_1 = 0$, (e) Inertial Amplifier Negative Mass (IANM) system obtained by considering $m_2 = 0$, (f) Inertial Amplifier (IA) system obtained by considering $m_1 = 0$ and $m_2 = 0$, (g) Negative Mass (NM) system obtained by considering $m_a = 0$ and $m_2 = 0$, (h) basic monoatomic system obtained by considering $m_a = 0$, $m_1 = 0$ and $m_2 = 0$	29
3.3	Displacement patterns for different types of responses (a) pure propagation (b) pure attenuation (c) fluctuating attenuation.	35
3.4	The figure corresponds to IANMNS system (given in Figure 3.2-(a)), with values of governing parameters $\theta = 1; \theta_{r1} = 3, \theta_{r2} = 0.25, \eta_{r2} = 2, \gamma = 1$ and varying η_{r1} from 0 to 5. The contour plot for frequency ratio η varying from 0 to 5 versus η_{r1} is shown in (e). In this figure (e) the silver, blue and green dashed lines depicts the roots of equations $Q(\eta^2) = 0$, $R(\eta^2) = 0$, and $R(\eta^2) + 2Q(\eta^2) = 0$ respectively. The (a), (b), (c) and (d) figures demonstrates the dispersion relation for the IANMNS system at sections drawn by pink lines at $\eta_{r1} = 0.5, 1.5, 2$ and 3.5 respectively.	44
3.5	IANMNS special case(with both the resonators with same frequencies ($\eta_{r1} = \eta_{r2}$)). system (given in Figure 3.2-(a)), with values of governing parameters $\theta = 1; \theta_{r1} = 3, \theta_{r2} = 0.25, \gamma = 1$ and varying $\eta_{r1} = \eta_{r2}$ from 0 to 5. The contour plot for frequency ratio η varying from 0 to 5 versus η_{r1} is shown in (e). In this figure (e) the silver, blue and green dashed lines depicts the roots of equations $Q(\eta^2) = 0$, $R(\eta^2) = 0$, and $R(\eta^2) + 2Q(\eta^2) = 0$ respectively. The (a), (b), (c) and (d) figures demonstrates the dispersion relation for the IANMNS special case system at sections drawn by pink lines at $\eta_{r1} = 0.5, 1.5, 2$ and 3.5 respectively.	45
3.6	NMNS system (given in Figure 3.2-(c)), with values of governing parameters $\theta_{r1} = 3, \theta_{r2} = 0.25, \eta_{r2} = 2, \gamma = 1$ and varying η_{r1} from 0 to 5. The contour plot for frequency ratio η varying from 0 to 5 versus η_{r1} is shown in (e). In this figure (e) the silver, blue and green dashed lines depicts the roots of equations $Q(\eta^2) = 0$, $R(\eta^2) = 0$, and $R(\eta^2) + 2Q(\eta^2) = 0$ respectively. The (a), (b), (c) and (d) figures demonstrates the dispersion relation for the NMNS system at sections drawn by pink lines at $\eta_{r1} = 0.5, 1.5, 2$ and 3.5 respectively.	46
3.7	IANM system (given in Figure 3.2-(e)), with values of governing parameters $\theta = 1, \theta_{r1} = 3, \gamma = 1$ and varying η_{r1} from 0 to 5. The contour plot for frequency ratio η varying from 0 to 5 versus η_{r1} is shown in (e). In this figure (e) the silver, blue and green dashed lines depicts the roots of equations $Q(\eta^2) = 0$, $R(\eta^2) = 0$, and $R(\eta^2) + 2Q(\eta^2) = 0$ respectively. The (a), (b), (c) and (d) figures demonstrates the dispersion relation for the IANM system at sections drawn by pink lines at $\eta_{r1} = 0.5, 1.5, 2$ and 2.75 respectively.	47

- 3.8 (a): System -IANS (given in Figure 3.2-(b)), (b): System -NS (given in Figure 3.2-(d)), (c): System -IA (given in Figure 3.2-(f)), (d): System -NM (given in Figure 3.2-(g)), Here silver, blue and green dashed lines are roots of equations $Q(\eta^2) = 0$, $R(\eta^2) = 0$, and $R(\eta^2) + 2Q(\eta^2) = 0$ respectively. 48
- 3.9 (a) Proposed hierarchical stiffness metamaterial comprising of hierarchical level resonators. (b) Demonstration of Koch curve construction started from level 1 (top), a straight line, to level 5 (bottom), a complex fractal shape from hierarchical triangles. (c) In similar manner, the evolution of the hierarchical stiffness metamaterial (HSM) is perceived. Level 1 of HSM (top) is same as a monoatomic chain which has a spring between two main masses. To construct a higher level HSM, a spring-mass-spring resonator is attached in parallel to the spring of the previous level. Both Koch curve and proposed HSM can be further extended to any level following the logic of the construction. 51
- 3.10 The nonzero values of stiffness matrix (\mathbf{K}) is shown for level two to five in respectively (a), (b), (c) and (d). 54
- 3.11 (a), (b) and (e) Dispersion diagram real and imaginary part of the propagation constant (κ) with respect to free wave frequency for $k_2 = 1$, $k_2 = 2$ and $k_2 = 3$ respectively. (c), (d) and (g) illustrate the variation of effective mass and stiffness with respect to free wave frequency. (f) the contour of attenuation level with the variation of stiffness k_2 . For all the plots $m_1 = 1$, $m_2 = 2$ and $k_1 = 1$. Blue, green and silver dashed lines are for bounds of band gaps obtained by roots of equations $R = 0$ and $2Q + R = 0$; and attenuation peaks obtained by equation $Q = 0$ respectively. 58
- 3.12 The stiffness and masses of level 6 are assumed to be $k = [k_1 \ k_2 \ k_3 \ k_4 \ k_5 \ k_6] = [0.001 \ 0.25 \ 0.5 \ 0.5 \ 0.6 \ 0.8]$ and $m = [m_1 \ m_2 \ m_3 \ m_4 \ m_5 \ m_6] = [1 \ 1.5 \ 2 \ 0.8 \ 0.5 \ 0.25]$; (a) Dispersion relation plot where, $\Re(\kappa)$ is phase angle of wave and $\Im(\kappa)$ is attenuation level of wave. BG1, BG2 and BG3 are considered band gaps with multiple peaks. (b),(c) and (d) are enlarged dispersion plot of three considered bandgaps which shows phenomenon of four attenuation peaks in all three bands. (e), (f) and (g) Effective mass (M_{eff}) is plotted for all three bandgaps. (h), (i) and (j) Effective stiffness (K_{eff}) is plotted for all three bandgaps and it has zero values at the exact location of attenuation peaks shown by green dashed lines. 62
- 4.1 (a) Monoatomic monocoupled chain, (b) Bicoupled chain with straight coupling, (c), Bicoupled chain with zigzag coupling, (d) Bicoupled chain with hybrid (straight and zigzag coupling), (e) Second order BNN type chain with additional mass, (f) Second order BNN type chain. 65
- 4.2 (a) Bicoupled chain with hybrid (straight and zigzag coupling), (b) Free body diagram of the representative unit cell. 66
- 4.3 The invariant plane ζ_2 versus ζ_1 . r and s lines are dotted lines which shows the boundaries of band structure. Moreover, p is dashed parabolic line depicts the complex band boundaries. PP, PA, AA and C are four regions for all four types of bands possible in any bicoupled system[9]. 71

4.4	Input parameters: $k_1 = 10000, k_2 = 2500, k_a = 500, k_c = 2500$. (A) Dispersion relation plot showing veering phenomenon, (B) Group velocity of propagating waves, (a-d) Mode of wave dispersion shown at frequencies given in (A) from different bands.	72
4.5	Input parameters: $k_1 = 10000, k_2 = 2500, k_a = 500, k_c = 10000$. (A) Dispersion relation plot showing wave locking-unlocking phenomenon, (B) Group velocity of propagating waves, (a-f) Mode of wave dispersion shown at frequencies given in (A) from different bands.	73
4.6	(A) symmetric representative unit cell of the metamaterial with three coupling degrees of freedom. a.1 and b.1 are respectively plots of real and imaginary values of propagation constant with respect to normalised frequency Ω for straight interconnection. Similarly, a.2 and b.2 are plots for zigzag interconnections.	75
4.7	Dispersion plot of multilayered spring mass chain of type A multicoupled system with k_a variation $k_a = \gamma k_2$, where $\gamma = [0, 0.1, 0.5, 1, 2, 2.5, 3.5, 4]$. . .	77
4.8	Dispersion plot of multilayered spring mass chain of type A multicoupled system with k_c variation $k_c = \gamma k_2$, where $\gamma = [0, 0.5, 1.0, 1.9, 2.1, 4.7, 7.4, 10]$. . .	78
4.9	Dispersion plot of multilayered spring mass chain of type A multicoupled system with k_a variation keeping k_c nonzero $k_a = \gamma k_2$, where $\gamma = [0, 1.7143, 3.4286, 5.1429, 6.8571, 8.5714, 10.2857, 12.0000]$ and $k_c = 6k_2$	80
4.10	Dispersion plot of multilayered spring mass chain of type A multicoupled system with k_c variation keeping k_c nonzero $k_c = \gamma k_2$, where $\gamma = [0.2, 0.6, 1.0, 1.4, 1.8, 2.2, 2.6, 3.0]$	81
4.11	Dispersion plot of multilayered spring mass chain of type A multicoupled system with $k_2 = 0, k_a = 0$ variation keeping k_c nonzero $k_c = \gamma k_1$, where $\gamma = [0.05, 0.1, 0.25, 0.5, 1.0, 2.0, 3.0, 4.0]$	83
5.1	(a) The Infinite Rigid Elastic combined meta(RECM) beam, (b) The representative unit cell of RECM beam (where, EI is flexural rigidity, A is area of cross section, l_1 and l_2 are lengths of elastic and rigid part of beam respectively, M is mass and J is rotary inertia of rigid body and L is total length of a unit cell)and (c) Free body diagram of unit cell of RECM beam (where, M_i and V_i are moment and shear force at i^{th} node, θ_c and y_c are slope and displacement at the center of rigid body).	87
5.2	Finite RECM beam chain.	92
5.3	Procedure for obtaining band characteristics and response in space-time domain for RECM beam.	94
5.4	(a) The representative unit cell of RECM beam for validation purpose and (b) Free body diagram of unit cell of RECM beam.	95
5.9	(a)Input excitation wave burst in time domain (b)Input excitation wave burst in frequency domain.	100

- 5.5 (a)Attenuation-profile for varying length ratio ξ having rotary inertia ratio $\psi = 0$ and mass ratio $\mu = 0.25$. For the system parameters corresponds to $\psi = 0$, $\mu = 0.25$ and $\xi = 1$ - (b) concise dispersion diagram illustrating the attenuation and propagation bands and (c) plot of the cross frequency response function evidenced the reduction of response in the attenuation band. The normalised band width of first and second band is 92.56% and 67.56% respectively. (d) Plot of logarithmic determinant of global Spectral element Matrix, where downward peak corresponds to the natural frequency of the system. The thin blue lines connecting resonance peaks in (c) and downward peak in (d) illustrate occurrence of resonance peaks in the stop band. The vertical black center line indicates the mid frequency ratio (12.5) for the wave burst for visualization of displacement in space time. 103
- 5.6 (a)Attenuation-profile for varying length ratio ξ having rotary inertia ratio $\psi = 5$ and mass ratio $\mu = 0.25$. For the system parameters corresponds to $\psi = 5$, $\mu = 0.25$ and $\xi = 0.56$ - (b) concise dispersion diagram illustrating the attenuation and propagation bands and (c) plot of the cross frequency response function evidenced the reduction of response in the attenuation band. The normalised band width of first merged band is 164.06% (d) Plot of logarithmic determinant of global Spectral element Matrix, where downward peak corresponds to the natural frequency of the system. The thin blue lines connecting resonance peaks in (c) and downward peak in (d) illustrate occurrence of resonance peaks in the stop band. The vertical black center line indicates the mid frequency ratio (12.5) for the wave burst for visualization of displacement in space time. 104
- 5.7 (a)Attenuation-profile for varying mass ratio μ having rotary inertia ratio $\psi = 5$ and length ratio $\xi = 0.5$. For the system parameters corresponds to $\psi = 5$, $\mu = 0.32$ and $\xi = 0.5$ - (b) concise dispersion diagram illustrating the attenuation and propagation bands and (c) plot of the cross frequency response function evidenced the reduction of response in the attenuation band. The normalised band width of first merged band is 163.41% (d) Plot of logarithmic determinant of global Spectral element Matrix, where downward peak corresponds to the natural frequency of the system. The thin blue lines connecting resonance peaks in (c) and downward peak in (d) illustrate occurrence of resonance peaks in the stop band. 105
- 5.8 (a)Attenuation-profile for varying rotary inertia ratio ψ having mass ratio $\mu = 5$ and length ratio $\xi = 0.5$. For the system parameters corresponds to $\psi = 1.71$, $\mu = 0.25$ and $\xi = 0.5$ - (b) concise dispersion diagram illustrating the attenuation and propagation bands and (c) plot of the cross frequency response function evidenced the reduction of response in the attenuation band. The normalised band width of second merged band is 136.14% (d) Plot of logarithmic determinant of global Spectral element Matrix, where downward peak corresponds to the natural frequency of the system. The thin blue lines connecting resonance peaks in (c) and downward peak in (d) illustrate occurrence of resonance peaks in the stop band. 106

5.10	(a)Wave propagation in space and time (b)snap shot of beam before the wave reaches connecting element (c) snap shot of beam after the wave propagates through connecting element; the red band shows the elastic(same material as of beam) connecting two elastic beams.	107
5.11	(a)Wave propagation in space and time (b) snap shot of beam before and (c) after the wave propagates through connecting element; the red band shows the RECM elements with zero rotary inertia- connecting two elastic beams.	108
5.12	(a)Wave propagation in space and time (b)snap shot of beam before the wave reaches connecting element (c) snap shot of beam after the wave propagates through connecting element; the red band shows the RECM elements with nonzero rotary inertia- connecting two elastic beams.	109
6.1	(a) CAD model of the REVI ; (b) 3D printing device; (c) 3D printed proposed REVI; (d) Analytically modeled REVI and (e) Degrees of freedom and boundary conditions at each node.	113
6.2	(a) Free vibration of REVI model for estimation of natural frequency; (b) Time acceleration plot of the free vibration analysis; (c) Frequency domain plots with the help of FFT algorithm (sensitivity of accelerometer = 4.98 mV/ms ⁻²).	126
6.3	Plot of determinant of dynamic stiffness matrix for natural frequency $\omega_n = 578.05$ rad/s with rotational spring stiffness k_r . The zero determinant is shown by a circle marker at the rotational stiffness $k_r = 0.3591$ Nm/rad.	126
6.4	(a) First, (b) Second and (c) Third modal shapes of REVI and (d) Logarithm of the determinant of spectral element matrix (\mathbf{K}_{bc}) of REVI.	127
6.5	(a) Power amplifier to vibrate the shaker system at desired gain and frequency; (b) REVI connected to the dynamic shaker system; (c) DAQ device used to collect the response of accelerometers and force transducers; (d) Simulation of data acquisition system using LabView software; (e) to (j) Time and frequency domain response of force transducers and accelerometers at a frequency of 92 Hz.	129
6.6	Transmittance of the proposed REVI system from experimental and analytical computation compared to an equivalent spring-mass system. The REVI system's bandwidth (shaded region) is 0.1767 for one-fourth amplitude transmittance.	132
6.7	Variation of Transmittance (T_r) with the excitation frequency for different mass ratios. (a) The mass $m_2 = 0$ and mass $m_3 = 2^p m_r$, where p varies from -1 to 3 , (b) The mass $m_2 = 2^q m_r$ and mass $m_3 = m_r$, where q varies from 2 to 6 , (c) The mass $m_2 = 2^q m_r$ and mass $m_3 = 2^p m_r$, where p varies from -2 to 2 and q varies from 2 to 6	134

- 6.8 Variation of transmittance (T_r) and relative transmittance's (T_{r1}) and (T_{r2}) with the excitation frequency for different mass ratios. The mass $m_1 = 2^q m_a$ and mass $m_2 = m_r$, where q increases from 0 to 2 (a) Transmittance $T_r = \log_{10}(\frac{u_2}{u_1})$, (b) Transmittance $T_{r1} = \log_{10}(\frac{u_3}{u_1})$, (c) Transmittance $T_{r2} = \log_{10}(\frac{u_3}{u_2})$ and transmittance $T_{r3} = \log_{10}(\frac{v_3}{u_2})$. The resonance in relative transmittance results in antiresonance in transmittance (T_r). 135
- 6.9 Effect of inclination angle on bandgap having node masses as 7.889×10^{-4} kg. (a) Transmittance plots for different values of inclination angle θ . (b) Attenuation profile (represented by negative values of transmittance plot) as a function of excitation frequency and inclination angle. In the attenuation band, double attenuation peaks can be obtained for inclination angles up to 33.41° . For $\theta = 33.42^\circ$, the two attenuation peaks merge to form a single attenuation peak. Further, an increment of the angle creates the resonance cancellation phenomenon, completely vanishing the attenuation peaks and further reducing the band gap. 136
- 6.10 Attenuation profile (represented by negative values of transmittance plot) as a function of excitation frequency and several geometric parameters such as (a) Length of the beam. (b) The thickness of the beam. (c) The mass ratio (ratio of the rigid mass to the primary mass of the system). 136
- 6.11 (a) Infinite chain of REVI, (b) Determinant of stiffness matrix with free-free boundary condition and fix-fix boundary condition, (c) Effective stiffness and Mass, and (d) Dispersion relation plot. vertical black dash dot lines connects the band boundaries with natural frequencies of unit cell and attenuation peaks with zero effective stiffness points. 139
- 6.12 Schematic and experimental setup of the REVI chain. (a) Diagram of a finite chain comprising nine REVI elements, (b) aluminum section used to fabricate the primary mass, (c) 3D-printed negative stiffness element with ends designed to fit into the aluminum section, (d) unit cell formed by combining the aluminum mass and the negative stiffness element, (e) complete chain of nine REVI units suspended from top rails, (f) close-up view of the ninth mass with an accelerometer, (g) close-up view of the first mass connected to the shaker via a stinger, with an accelerometer. 140
- 6.13 Steady-state vibration response of the REVI chain at 70 Hz. (a) Time histories for base acceleration, acceleration at node 1 (A_1), and acceleration at node 9 (A_9), respectively. (b) Corresponding FFT plots for the base, node 1, and node 9 accelerations. 141
- 6.14 Vibration transmittance across nodes of the REVI chain. (a) Transmittance at node 1, (b) transmittance at node 5, and (c) transmittance at node 9. Solid lines represent analytical predictions, while circular markers indicate experimental measurements. 142
- 7.1 (a) The Euler Bernoulli beam periodically supported by nonlinear springs (b) The representative unit cell 146

- 7.2 (a) The long Euler Bernoulli beam with $c_1 = c_2 = 0, k_3 = -1, k_1 = 1, A = 1, \epsilon = 0.1$, (b) Displacement contour of the middle portion of the beam shown by the dashed box, (c) Displacement versus distance plot at different instances of time shown in horizontal dashed lines with orange shades in (b), (d) Displacement versus time plot at different locations shown in vertical dashed lines with violet shades in (b), (e) FFT plots corresponding to displacement profiles shown in (c), (f) FFT plots corresponding to time histories shown in (d). 153
- 7.3 (a) Displacement contour of the Euler Bernoulli beam with $c_1 = c_2 = 0.05, k_3 = 1, k_1 = 1, A = 0.1, \epsilon = 1$; (b) Displacement versus time plot at different locations shown in vertical dashed lines with violet shades in (a) where the solid lines depict numerical solution and the dashed lines depict analytical solution, moreover the magnified plots are shown inside to showcase the better validation in the initial time window and degraded validation in later time window; (c) Displacement versus distance plot at different instances of time shown in horizontal dashed lines with orange shades in (a); (d) FFT plots corresponding to displacement profiles shown in (c). 154
- 7.4 (a) Dispersion relation plot for undamped system with $c_1 = c_2 = 0, k_1 = 1$ and nonlinear stiffness parameter $k_3 = -1, 0$ and 1 ; (b) Phase portrait for propagation constant $\kappa = 0.5$; (c) displacement profile for $\kappa = 0.5, k_3 = -1$; (d) displacement profile for $\kappa = 0.5, k_3 = 0$; (e) displacement profile for $\kappa = 0.5, k_3 = 1$; (f) Displacement time history at middle node of the beam with $\kappa = 0.5, k_3 = -1$; (g) Displacement time history at the middle node of the beam with $\kappa = 0.5, k_3 = 0$; (h) Displacement time history at the middle node of the beam with $\kappa = 0.5, k_3 = 1$ 155
- 7.5 (a) Dispersion relation plot for the undamped system with $c_1 = c_2 = 0, k_1 = 1, k_3 = 1$; (b) Phase portrait for propagation constant $\kappa = 0.25, 1.00$ and 1.75 ; (c) displacement profile for $\kappa = 0.25, k_3 = 1$; (d) displacement profile for $\kappa = 1.00, k_3 = 1$; (e) displacement profile for $\kappa = 1.75, k_3 = 1$; (f) Displacement time history at middle node of the beam with $\kappa = 0.25, k_3 = 1$; (g) Displacement time history at middle node of the beam with $\kappa = 1.00, k_3 = 10$; (h) Displacement time history at middle node of the beam with $\kappa = 1.75, k_3 = 1$. 156
- 7.6 Dispersion relation plots at different time instances are illustrated for hardening system with blue shades and softening system with shades of pink for (a) only viscous damping $c_1 = 0.25$ and $c_2 = 0$, (b) only strain rate damping $c_1 = 0$ and $c_2 = 0.25$ and (c) viscous damping and strain rate damping $c_1 = 0.25$ and $c_2 = 0.25$; Frequency shift versus propagation constant (κ) plots at different time instances are illustrated for hardening system with blue shades and softening system with shades of pink for (d) only viscous damping $c_1 = 0.25$ and $c_2 = 0$, (e) only strain rate damping $c_1 = 0$ and $c_2 = 0.25$ and (f) viscous damping and strain rate damping $c_1 = 0.25$ and $c_2 = 0.25$ 157
-

List of Tables

3.1	Closed form solution of the roots of the governing polynomials. The labels in first column corresponds to the systems given in Figure 3.2(a-h)	40
3.2	Input data for validation	41
3.3	Attenuation characteristics as per literature(lit*) and proposed(pro*) method	42
3.4	Systems and the values of their governing nondimensional parameters with possibility of double peak phenomenon. The labels in first column corresponds to the systems given in Figure 3.2(a-h)	43
3.5	The generalised degrees of rational polynomials of dispersion for N level HSM hierarchy	57
3.6	The value of the effective mass, effective stiffness and Q , R and $2Q + R$ polynomial at the frequencies ψ_1, ξ_1 and ξ_2 as evaluated in Eq 3.81 and 3.82	60
4.1	Types of dispersion bands in bicoupled system as per propagation constant (κ)	70
5.1	Natural frequency ω_n for combined elastic rigid beam with properties - $l_1 = 0.8L$, $l_2 = 0.2L$, $l_3 = 0.3L$, $\psi = 0$, $\mu = 0.5$ and $\xi = 0.5$	96
6.1	Material and Geometrical properties	112

ABBREVIATIONS

1D	One Dimensional
BS	Bragg Scattering
dof	degrees of freedom
HSM	Hierarchical Stiffness Metamaterial
IA	Inertial Amplifier
NM	Negative Mass
NS	Negative Stiffness
IANM	Inertial Amplifier Negative Mass
IANS	Inertial Amplifier Negative Stiffness
IANMNS	Inertial Amplifier Negative Mass Negative Stiffness
NMNS	Negative Mass Negative Stiffness
LR	Local Resonance
RECM	Rigid Elastic Combined Metabeam
REVI	Rigid Elastic Vibration Isolator

List of symbols

ω	Excitation frequency
η	Frequency ratio
κ	Propagation constant
$\Re(\kappa)$	Real part of propagation constant
$\Im(\kappa)$	Imaginary part of propagation constant
EI	Flexural rigidity
ρ	Density
A	Area of cross section
M_{eff}	Effective mass
K_{eff}	Effective stiffness
t	Time
a_0	amplitude
ϵ	Book-keeping parameter
v_g	Group velocity
ι	Influence vector
ξ	Length ratio
μ	Mass ratio
ψ	Rotary inertia ratio
M	Mass
K	Stiffness
k_g	Global stiffness matrix
ζ	Invariants
k_a	Stiffness of straight coupling
k_c	Stiffness of zigzag coupling
m_a	Mass of inertial amplifier mechanism

m_r	Rigid mass
J_r	Rigid body polar moment of inertia
M_a	Mass of accelerometer
T_r	Transmittance
D_y	Dynamic Stiffness matrix
C_s	Strain rate dependent damping
C_a	Velocity dependent viscous damping
x	Distance
t	Time
\tilde{k}_1	Linear spring
\tilde{k}_3	Nonlinear spring
l	Length of beam
Π	Nonlinearity factor
ψ	Shape function
ω_n	Natural frequency
